Preliminary Results with a Low-Cost Fiber-Optic Gyrocompass System

Andrew R. Spielvogel and Louis L. Whitcomb

***Abstract*— This paper reports results of preliminary numerical simulation studies and preliminary static experimental evaluation of a true-North gyrocompass system employing a commercially available low-cost inertial measurement unit (IMU) comprising a 3-axis fiber optic gyroscope (FOG) with micro-electro-mechanical systems (MEMS) accelerometers. North-seeking gyrocompass systems typically employ a microprocessor system to sample the IMUs low-level raw sensor values for angular-rate and linear-acceleration at a high sampling rate, compensate for sensor bias and alignment, and compute a high-level estimate for true-North heading, pitch, and roll. We report the results of a numerical simulation study to evaluate the potential accuracy of the proposed system, and a numerical sensitivity study to evaluate how this accuracy will change with variation in the sensor measurement noise of the gyroscopes and accelerometers. We report preliminary experimental results for a static benchtop configuration of this system which utilizes 3-axis angular-rate data and 3-axis linear acceleration sensor data to estimate the instrument's 3-degrees of freedom (DOF) attitude (heading, pitch, and roll) without using magnetometry of the Earth's magnetic field. These preliminary results for a static benchtop IMU configuration are promising, and directly applicable to static instrument deployments, but further development, testing, and evaluation is needed for the case of dynamic IMU configuration typically found on moving marine vehicles.**

I. Introduction

Over the past decade, the development of a new generation of small low-cost underwater vehicles (UVs) has begun to enable oceanographic, environmental assessment, and national security missions that were considered impractical or infeasible before (e.g. [1], [2], [6], [7], [10]). This new generation of UVs often employ low-cost navigation systems that presently limit them to missions requiring only low-precision navigation of $\mathcal{O}$(10-100)m accuracy. High-end navigation approaches, of $\mathcal{O}$(0.1-10)m accuracy, traditionally require a Doppler sonar, costing \$20K-\$50K, and a North-seeking gyrocompass or inertial navigation system (INS), costing \$50K-\$250K. These high-end navigation approaches are largely incompatible with low-cost autonomous underwater vehicles (AUVs) with target total vehicle cost of \$50k-\$250K.

Small low-cost UVs typically employ micro-electro-mechanical systems (MEMS) inertial measurement units (IMUs) comprised of 3-axis MEMS magnetometers and 3-axis MEMS accelerometers to estimate local magnetic heading, pitch, and roll to within several degrees of accuracy. Studies have shown that the accuracy of these magnetic heading sensors can be a principal error source in overall navigation solutions [4].

These low-accuracy attitude sensors limit the navigation accuracy of small vehicles for scientific and military survey missions such as high-resolution optical and acoustic imaging, mine countermeasures, and multibeam acoustic hydrography. The high cost, large size, and high power-consumption of conventional mechanical and optical true-North seeking gyrocompasses is a principal barrier to the widespread use of high accuracy navigation for smaller and lower-cost UVs.

This paper reports the results of preliminary simulations and preliminary static experimental evaluation of a system employing a comparatively low-cost commercial-off-the-shelf (COTS) KVH 1775 IMU (KVH Industries, Inc., Middletown, RI, USA) for estimation of true-North heading, pitch and roll. The true-North estimates derived from the KVH 1775 IMU data are compared with the true-North heading output provided by an iXBlue PHINS INS (iXBlue SAS, Marley le Roi, France).

The KVH 1775 IMU draws about 5 W, weighs 0.7 kg, and its roughly cylindrical housing is approximately 96 mm in diameter $\times$ 74 mm in height [5]. The iXBlue PHINS INS draws under 20 W, weighs 4.5 kg, and its rectangular housing measures approximately 180 mm $\times$ 180 mm $\times$ 162 mm [3]. The PHINS is an excellent high-end INS providing a dynamic heading accuracy of 0.01 $^\circ \cdot$ secant(latitude) when GPS correction is available, [3], and a dynamic heading accuracy of 0.05$^\circ \cdot$ secant(latitude) with no external correction (our test configuration) — and thus can serve as an excellent "ground truth" comparison for these studies. Figure 1 depicts these two instruments.

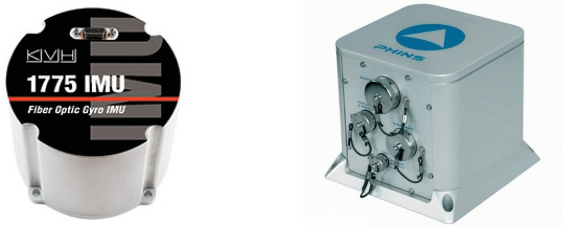

(a) KVH 1775 IMU (b) iXBlue PHINS INS

Fig. 1. Vehicle Attitude Estimation: (a) The KVH 1775 IMU; (b) The iXBlue PHINS INS employed in this study. (Note: Not to scale.)

This paper is organized as follows: Section II gives an overview of the coordinate frame conventions used in this paper. Section III reports a numerical sensitivity analysis of true-North heading error due to Gaussian sensor measure-

We gratefully acknowledge the support of the National Science Foundation under NSF award OCE-1435818. The authors are with the Department of Mechanical Engineering, Johns Hopkins University, Baltimore, MD 21218, USA. Email: {aspielv1,llw}@jhu.edu

978-0-933957-43-5

ment noise arising in angular rate measurements of the 3-axis gyroscopes and the 3-axis accelerometers. Section IV reports the results of preliminary laboratory experiments to evaluate the performance of the KVH 1775 IMU sensor as the primary sensor in a North-seeking gyrocompass system for the case of a static benchtop IMU configuration, with simple sensor bias calibration and compensation. Section V summarizes and concludes.

II. Coordinate Frames

A. Notation

For each vector, a leading superscript indicates the frame of reference and a following subscript indicates the signal source, thus ${}^{e}p_i$ is the instrument position in Earth coordinates, ${}^{N}w_i$ is the gyroscope angular velocity in the North-East-Down (NED) frame, and ${}^{i}a_i$ is the accelerometer linear acceleration in the instrument sensor frame.

The x, y, and z elements of a vector are represented by subscripts. For example, ${}^{s}w_{e,x}$, ${}^{s}w_{e,y}$, and ${}^{s}w_{e,z}$ are the x, y, and z components respectively of the angular velocity of the Earth in the star frame.

The set of 3×3 rotation matrices forms a group, known as the special orthogonal group, SO(3), defined as

$$SO(3) = \{R : R \in \mathbb{R}^{3\times3}, R^T R = I, det(R) = 1\}. \quad (1)$$

For each rotation matrix a leading superscript and subscript indicates the frames of reference. For example, ${}^{N}_{i}R$ is the rotation from the instrument frame to the NED frame.

B. Coordinate Frames

We define the following coordinate frames [8]:

Star Frame: The star frame has its origin at the center of the Earth, with its axes fixed (non-rotating) with respect to the stars, and with its z-axis aligned with the Earth's axis of rotation. For the purpose of this analysis the star frame can be considered an inertial reference frame.

Earth Frame: The Earth frame has its origin at the center of the Earth, with its axes fixed (non-rotating) with respect to the Earth, and with its z-axis aligned with the Earth's axis of rotation. The Earth frame rotates with respect to the star frame about their coincident z-axes at the Earth's rotation rate of $+15^\circ$ per hour.

North-East-Down (NED) Frame: The NED frame has its origin fixed on the surface of the Earth at the location of the instrument, with its x-axis pointing North, its y-axis pointing East, and its z-axis pointing down. The NED frame also rotates with respect to the star frame at the Earth's rotation rate of $+15^\circ$ per hour.

Instrument Frame: A frame fixed in the IMU instrument.

The time varying rotation transformation of instrument frame to star frame can be written as

$${}^{s}_{i}R = {}^{s}_{e}R\,{}^{e}_{N}R\,{}^{N}_{i}R \quad (2)$$

where ${}^{e}_{N}R$ is dependent on the instrument's location on Earth, ${}^{N}_{i}R$ is dependent on instrument rotation, and

$${}^{s}_{e}R = e^{{}^{s}\hat{w}_e t} \quad (3)$$

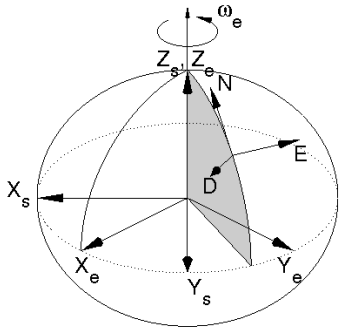

Fig. 2. The star frame (s), Earth frame (e), and North-East-Down frame (N). w_e is the Earth's angular velocity with a magnitude of +15°/hr.

where t is time and ${}^{s}\hat{w}_e$ is the skew symmetric matrix of the Earth's angular velocity, ${}^{s}w_e$ = [0,0,15°/hr]^T, and

$${}^{s}\hat{w}_e = \widehat{\begin{bmatrix} 0 \\ 0 \\ 1 \end{bmatrix}} (15^\circ/\text{hr}) \quad (4)$$

$$= \begin{bmatrix} 0 & -1 & 0 \\ 1 & 0 & 0 \\ 0 & 0 & 0 \end{bmatrix} (15^\circ/\text{hr})\,. \quad (5)$$

C. Static True-North Calculation

North-seeking gyrocompasses sense the Earth's rotation and gravitational field to determine directly the local vertical and true-North. For this paper, we assume the static case where the instrument is fixed to the lab benchtop, hence it is not moving or rotating with respect to the Earth frame. Since the instrument is static, it experiences a constant angular velocity due to the Earth's rotation and a constant linear acceleration due to gravity. By averaging sensor samples, we obtain estimates for the instrument frame angular velocity and linear acceleration

$${}^{i}\bar{w}_i = \left(\sum_{m=1}^{n} {}^{i}w_{i,m}\right)/n \quad (6)$$

$${}^{i}\bar{a}_i = \left(\sum_{m=1}^{n} {}^{i}a_{i,m}\right)/n \quad (7)$$

where ${}^{i}\bar{w}_i$ is the estimated instrument angular velocity, ${}^{i}w_{i,m}$ are the individual gyroscope sensor readings, ${}^{i}\bar{a}_i$ is the estimated linear acceleration, and ${}^{i}a_{i,m}$ are the individual accelerometer sensor readings. Estimates for the NED frame in instrument frame coordinates can be found by taking cross-products

$${}^{i}d = -\frac{{}^{i}\bar{a}_i}{\|{}^{i}\bar{a}_i\|}, \quad (8)$$

$${}^{i}e = {}^{i}d \times \frac{{}^{i}\bar{w}_i}{\|{}^{i}\bar{w}_i\|}, \quad (9)$$

$${}^{i}n = {}^{i}e \times {}^{i}d \quad (10)$$

where ${}^{i}n$, ${}^{i}e$, ${}^{i}d$ are NED unit vectors, respectively, in the instrument frame. Thus,

$${}^{N}_{i}R = \begin{bmatrix} {}^{i}n & {}^{i}e & {}^{i}d \end{bmatrix}^T. \quad (11)$$

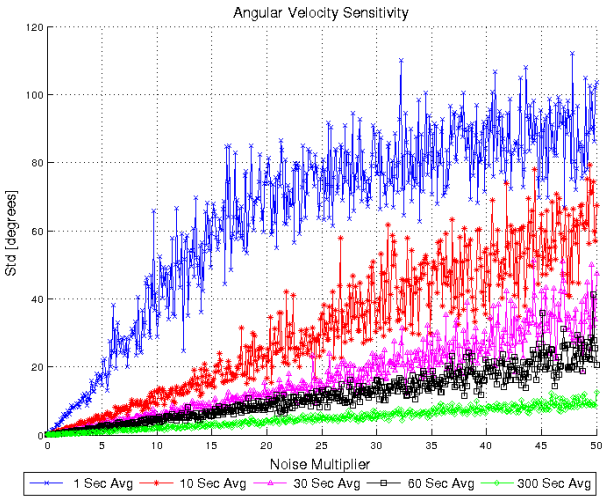

(a) Heading error standard deviation and noise multiplier relation.

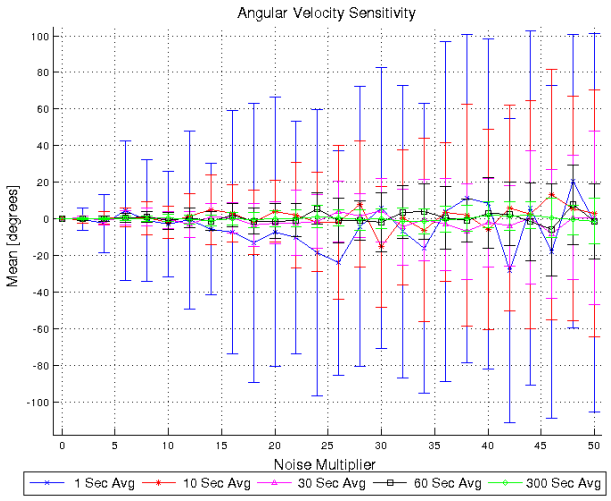

(b) Heading error mean and error bars as a function of noise multiplier.

Fig. 3. True-North heading sensitivity to gyroscope sensor noise. Shows 5 different sample averaging lengths for 0 to 50 noise multipliers.

III. Numerical Sensitivity Analysis

A. Numerical Sensitivity Analysis in Simulation

The sensor data is modeled as

$$ {}^{i}w_i = {}^{i}w_e + {}^{i}w_{vehicle} + {}^{i}w_{bias} + {}^{i}\eta_w \quad (12) $$

$$ {}^{i}a_i = {}^{i}a_g + {}^{i}a_{vehicle} + {}^{i}a_{bias} + {}^{i}\eta_a \quad (13) $$

where ${}^{i}w_i$ is the IMU measured angular-rate, ${}^{i}w_e$ is the true angular velocity due to the rotation of the earth, ${}^{i}w_{vehicle}$ is the true angular velocity due to the rotation of the vehicle with respect to the Earth frame, ${}^{i}w_{bias}$ is the angular velocity sensor bias offset, ${}^{i}\eta_w$ is zero-mean Gaussian angular velocity sensor noise, ${}^{i}a_i$ is the IMU measured linear acceleration, ${}^{i}a_g$ is the acceleration due to gravity, ${}^{i}a_{vehicle}$ is the vehicle's linear acceleration with respect to the Earth frame, ${}^{i}a_{bias}$ is the linear accelerometer sensor bias, and ${}^{i}\eta_a$ is zero-mean Gaussian linear accelerometer sensor noise. Our calculations for the angular velocity sensor and linear accelerometer sensor noises were computed from the IMU manufacturer's specifications [5] as per [9]. For this paper, the IMU data was sampled at 1000 Hz, which corresponds to $\sigma_w = 6.32 \times 10^{-3\circ}/\text{s}$ and $\sigma_a = 6.57$ mg where σ_w and σ_a are, respectively, the standard deviations of the normally distributed zero mean gyroscope and accelerometer sensor noise.

We assume that the instrument is fixed on the face of the earth, ${}^{i}w_{vehicle} = {}^{i}a_{vehicle} = 0$, and that the bias offset has been accurately estimated and compensated. With these assumptions, the model simplifies to

$$ {}^{i}w_i = {}^{i}w_e + {}^{i}\eta_w \quad (14) $$

$$ {}^{i}a_i = {}^{i}a_g + {}^{i}\eta_w \quad (15) $$

To determine the sensitivity of the true-North heading error to accelerometer and gyroscope noise, we ran numerical simulations varying the simulated accelerometer and gyroscope noise. We compared the heading error standard deviation and mean of 30 ensembles as the KVH 1775 IMU noise characteristics (shown in Table I, [5]) were multiplied by "noise multiplier" factors ranging from 0 to 50. This analysis was computed for five different sample averaging periods (1, 10, 30, 60, 300 seconds). The simulations were computed with the simulated location of the instrument at the same latitude on Earth as Johns Hopkins University (39.3289° N) for comparison with our experimental data.

TABLE I
KVH 1775 IMU Accelerometer and Gyroscope Specifications [5]

Sensor	Variable	Specification
Gyroscope	Bias Instability ($25°C$)	$\leq 0.1°$/hr, 1σ (max), $\leq 0.05°$/hr, 1σ (typical)
	Bias Offset ($25°C$)	$\pm 0.5°$/hr
	Angle Random Walk ($25°C$)	$\leq 0.012°/\sqrt{\text{hr}}$
Accelerometer	Bias Instability (constant temp)	< 0.05 mg, 1σ
	Velocity Random Walk ($25°C$)	≤ 0.12 mg/$\sqrt{\text{Hz}}$

B. Sensitivity to Angular Velocity Noise

The simulations show that the angular velocity sensor noise has a significant effect on true-North heading error. As shown in Figure 3(a), an increase in noise leads to the degradation of the heading estimate. Figure 3(b) shows how the mean heading error centers around zero degrees while the standard deviation error bars grow as the noise multiplier is increased. Figure 5 shows a portion of Figure 3(a), illustrating the simulated performance of the KVH 1775 IMU as a true-North Heading estimator about the published noise specifications [5] (noise multiplier of 1). From Figure 5, we see that, ideally, the KVH 1775 IMU data should give rise to a heading error standard deviation of less than 1° when averaging more than 30 seconds of data.

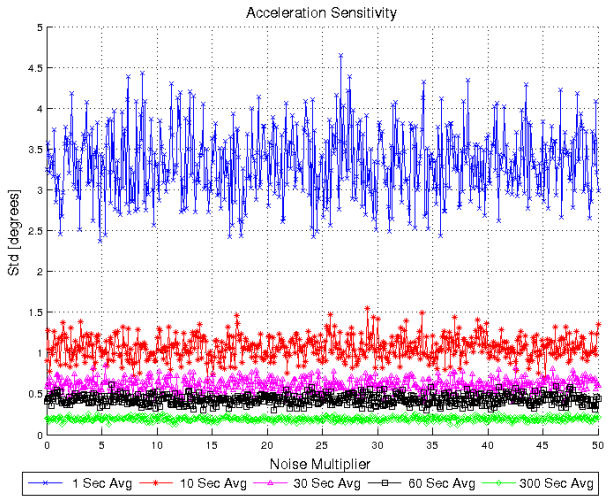

(a) Heading error standard deviation and noise multiplier relation.

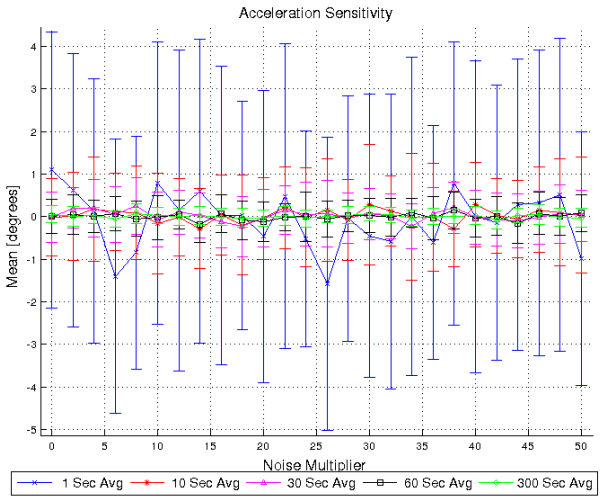

(b) Heading error mean and error bars as a function of noise multiplier.

Fig. 4. True-North heading sensitivity to linear accelerometer sensor noise. Shows 5 different sample averaging lengths for 0 to 50 noise multipliers.

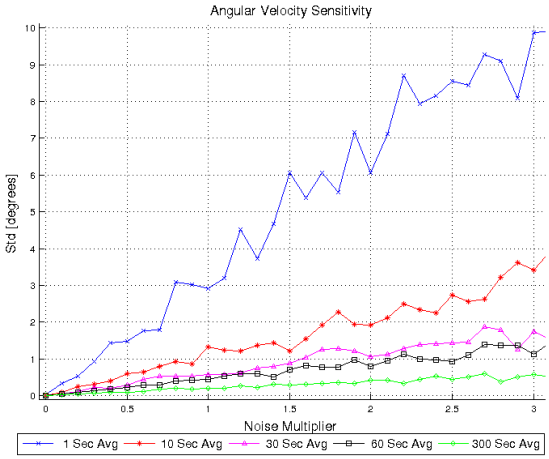

Fig. 5. Portion of Figure 3(a) showing the heading error standard deviation and noise multiplier relation for noise multipliers of 0 to 3.

C. Sensitivity to Acceleration Noise

Simulations altering the noise multiplier on the linear acceleration sensor noise of the KVH 1775 IMU show that linear acceleration sensor noise with up to a 50 noise multiplier has negligible effect on the true-North heading estimation. As shown in Figure 4(a), the standard deviation of the heading error for the simulation trials remains constant for accelerometer noise multipliers ranging from 0 to 50. The large magnitude of the gravity vector dominates the linear accelerometer sensor noise, mitigating the effect of the noise on the local level estimate and, hence, true-North heading estimate.

IV. Experiments and Results

A. Experimental Setup

We experimentally evaluated the accuracy of the true-North heading estimate arising from data obtained from a KVH 1775 IMU by comparing the resulting heading estimate to that of an iXBlue PHINS INS. In this experiment, the two instruments were co-located on a machined benchtop fiducial plate, located with dowel pins such that the instrument coordinate systems of the two instruments were aligned.

Before running experiments, a sensor bias estimation calibration was performed as follows:

1) The two instruments were powered on and allowed to warm up for 30 minutes. This warm-up period gave the iXBlue PHINS INS much more than enough time to find true-North with a dynamic heading accuracy of $\leq 0.05°/\cos(\text{latitude})$ when in our test configuration in which it was not receiving external corrections. The warm-up period allowed for the KVH 1775 IMU to stabilize to a constant operating temperature. This stable operating temperature of the IMU was important because the sensor biases of gyroscopes and linear accelerometers can vary with temperature.
2) After the warm-up period, five minutes of KVH 1775 IMU sensor data from three different orientations was recorded. The orientations are defined as followed:
   - **XY Orientation (xy):** The x-y plane of the KVH 1775 IMU is aligned with the local level of the iXBlue PHINS INS and the z-axis of the IMU up.
   - **XY Rotated Orientation (xy_rot):** The xy orientation rotated 180° around the z-axis.
   - **Z Down Orientation (z_down):** The instrument is inverted so that the x-y plane of the IMU is aligned with the local level of the INS and the z-axis of the IMU down.
3) The three sets of five minute sensor calibration data were used to calculate an estimate of the gyroscope and linear accelerometer bias offsets. The recorded sensor readings from each orientation were averaged to generate mean angular-rate and linear acceleration signal vectors for each orientation. The mean signal vectors were combined to estimate the gyroscope and

accelerometer's bias offsets:

$$ {}^{i}w_{bias} = \left(\frac{1}{2}\right) \begin{bmatrix} {}^{xy}\bar{w}_{i,x} + {}^{xy\_rot}\bar{w}_{i,x} \\ {}^{xy}\bar{w}_{i,y} + {}^{xy\_rot}\bar{w}_{i,y} \\ {}^{xy}\bar{w}_{i,z} + {}^{z\_down}\bar{w}_{i,z} \end{bmatrix} \quad (16) $$

$$ {}^{i}a_{bias} = \left(\frac{1}{2}\right) \begin{bmatrix} {}^{xy}\bar{a}_{i,x} + {}^{xy\_rot}\bar{a}_{i,x} \\ {}^{xy}\bar{a}_{i,y} + {}^{xy\_rot}\bar{a}_{i,y} \\ {}^{xy}\bar{a}_{i,z} + {}^{z\_down}\bar{a}_{i,z} \end{bmatrix} \quad (17) $$

where ${}^{xy}\bar{w}_i$, ${}^{xy\_rot}\bar{w}_i$ and ${}^{z\_down}\bar{w}_i$ are the xy, xy_rot and z_down orientations' mean angular velocity signal vectors, respectively, and ${}^{xy}\bar{a}_i$, ${}^{xy\_rot}\bar{a}_i$ and ${}^{z\_down}\bar{a}_i$ are the xy, xy_rot and z_down orientations' mean linear acceleration signal vectors, respectively.

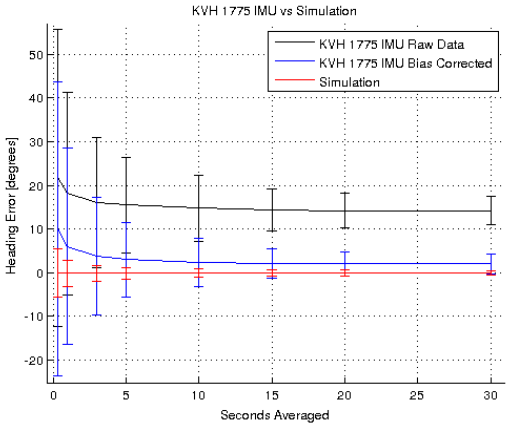

Fig. 6. Comparison of the experimentally observed heading error mean and standard deviation data to simulated heading error calculations.

B. Experimental Heading Accuracy

KVH 1775 IMU sensor data was recorded for ∼53 minutes. Using the sensor biases calculated per (16)-(17), the raw sensor data was corrected by subtracting out the bias offset:

$$ {}^{i}\tilde{w}_i = {}^{i}w_i - {}^{i}w_{bias} \quad (18) $$

$$ {}^{i}\tilde{a}_i = {}^{i}a_i - {}^{i}a_{bias} \quad (19) $$

where ${}^{i}\tilde{w}_i$ and ${}^{i}\tilde{a}_i$ are the corrected angular velocity and linear acceleration data respectively. Figure 6 shows the calculated experimentally observed mean heading error and standard deviation for the recorded sensor readings, bias-corrected sensor readings, and simulation. Examination of the heading error for the recorded raw (uncorrected) and bias-corrected samples in Figure 6 shows that the sensor bias offsets drastically affect the true-North estimate. The mean heading error from raw uncorrected data is ∼15°, and ∼2° for the bias-corrected data. While it was fully expected that the raw sensor data (uncorrected for bias) would give rise to a biased heading estimate, it was not expected that the bias-corrected sensor data would also consistently give rise to a biased heading estimate. We conjecture that this may be the result of an inadequate bias calibration method, or other effects such as non-orthogonality of the individual sensor channels for the fiber optic gyroscopes (FOGs) and the accelerometers for which we did not calibrate in this preliminary study.

V. Conclusions

This paper reports preliminary simulation and preliminary experimental evaluation of a commercially available low-cost IMU for true-North heading estimation for a static IMU configuration. The results indicate that a system employing low-cost FOG IMUs can successfully find true-North. The simulations and Figure (5) suggest that the low-cost KVH 1775 IMU, according to its specifications, should be capable of being employed in a system to find true-North with within an accuracy of 1°. In addition, the sensitivity analysis in Section III suggests gyroscope sensor noise is a principal source of error for North-seeking heading estimates.

In addition to gyrocompass sensor noise, inaccurate sensor bias offset calibration biases the heading estimation. Our current method for calculating sensor bias offset provides an improvement over no bias compensation in heading error. However, improved bias and alignment calibration methods may improve the accuracy of the gyrocompass bias offset calculation.

Overall, these data suggest practical utility of low-cost commercially available FOG IMUs as the primary sensor in a North-seeking gyrocompass system for the case of a static benchtop IMU configuration. In future studies, we hope to address the case of dynamic instrument motion in both translation and rotation.

References

[1] D. Clegg and M. Peterson. User operational evaluation system of unmanned underwater vehicles for very shallow water mine countermeasures. In *OCEANS 2003. Proceedings*, volume 3, pages 1417–1423 Vol.3, Sept 2003.

[2] T. Clem, D. Sternlicht, J. Fernandez, J. Prater, R. Holtzapple, R. Gibson, J. Klose, and T. Marston. Demonstration of advanced sensors for underwater unexploded ordnance (UXO) detection. In *Oceans, 2012*, pages 1–4, Oct 2012.

[3] IXBLUE, SAS, Marley Le Roi, France. The IXBLUE web site http://www.ixsea.com and PHINS specification sheet http://www.ixsea.com/pdf/br-phins-2012-02-web.pdf.

[4] J. C. Kinsey and L. L. Whitcomb. Preliminary field experience with the DVLNAV integrated navigation system for oceanographic submersibles. *Control Engineering Practice*, 12(12):1541–1548, December 2004. Invited Paper.

[5] KVH Industries, Inc., Middletown, RI, USA. The KVH web site http://www.kvh.com and KVH 1775 IMU specifications sheet http://www.kvh.com/viewattachment.aspx?guidid=DFB3BCDF-CFA1-422D-837A-92F4F68D9BE5.

[6] G. Packard, A. Kukulya, T. Austin, M. Dennett, R. Littlefield, G. Packard, M. Purcell, R. Stokey, and G. Skomal. Continuous autonomous tracking and imaging of white sharks and basking sharks using a REMUS-100 AUV. In *Oceans - San Diego, 2013*, pages 1–5, Sept 2013.

[7] E. Steele, T. Boyd, M. Inall, E. Dumont, and C. Griffiths. Cooling of the West Spitsbergen Current: AUV-based turbulence measurements west of Svalbard. In *Autonomous Underwater Vehicles (AUV), 2012 IEEE/OES*, pages 1–7, Sept 2012.

[8] D. Titterton, J. Weston, J. Weston, and I. of Electrical Engineers. *Strapdown inertial navigation technology*. IEE radar, sonar, navigation, and avionics series. Peter Peregrinis Ltd. on behalf of the Institution of Electrical Engineers, 1997.

[9] Woodman, Oliver J. An introduction to inertial navigation. Technical report, University of Cambridge, Cambridge, UK, 2007.

[10] M. Zhou, R. Bachmayer, and B. de Young. Working towards seafloor and underwater iceberg mapping with a Slocum glider. In *Autonomous Underwater Vehicles (AUV), 2014 IEEE/OES*, pages 1–5, Oct 2014.